Tethering Effects in Oligomer-Based Metal–Organic Frameworks

*Ryan A. Dodson,[1] Junkil Park,[2] Jihan Kim,[2] Matthew J. Cliffe,[3] and Seth M. Cohen[1]**

[1]Department of Chemistry and Biochemistry, University of California, San Diego, La Jolla, California 92093, USA

[2]Department of Chemical and Biomolecular Engineering, Korea Advanced Institute of Science and Technology (KAIST), Daejeon 34141, South Korea

[3]School of Chemistry, University of Nottingham, University Park, Nottingham, NG7 2RD, United Kingdom

KEYWORDS: crosslinked MOFs, metal–organic frameworks, oligoMOFs, polymer–MOF hybrids, polyMOFs

ABSTRACT. Metal-organic frameworks (MOFs) can be constructed using conventional molecular linkers or polymeric linkers (polyMOFs), but the relationship and relative properties of these related materials remains understudied. As an intermediate between these two extremes, a library of oligomeric ligand precursors (dimers, trimers) was used to prepare a series of oligomeric-linker MOFs (oligoMOFs) based on the prototypical IRMOF-1 system. IRMOF-1 was found to be remarkably tolerant to a wide variety of oligomeric linkers, the use of which greatly enhanced MOF yield and prevented framework interpenetration. Tether length-dependent ordering of ligand and metal cluster orientations was also observed in these 'oligoMOFs'. Improved low-humidity stability was found in oligoIRMOF-1 samples, with surface area preservation varying as a function of tether length, and a complete suppression of crystalline hydrolysis products for all oligoIRMOF-1 materials studied. These findings pave the way toward a better understanding of the structure-function relationships present in monomeric, oligomeric, and polymeric MOFs, and highlight an underutilized strategy for tuning MOF properties.

INTRODUCTION

Metal–organic frameworks (MOFs) are a class of materials comprising metal ions or clusters bound by multitopic organic linkers to generate crystalline, porous structures.[1] MOFs have been extensively studied and proposed for applications including sensing, separations, storage, and catalysis.[2] While MOFs can often excel in laboratory studies of these applications under controlled conditions, their more widespread adoption has been hindered by a number of factors. Chief among these is that MOFs created using yield-optimized syntheses generally take the form of microcrystalline powders,[3-5] which contain significant interparticle void volume and cannot be easily converted into freestanding membranes or fibers. To address this inherent challenge, many studies have explored MOF–polymer composite materials.[6] These hybrid composites have the potential to demonstrate the best features of both materials: the high surface areas and well-defined pore chemistry of MOFs, and the processibility and excellent mechanical properties (strength, toughness, elasticity) of polymers.

PolyMOFs, which are MOFs synthesized from polymer linkers (i.e., using ligand units pre-tethered together via covalent spacers) instead of molecular linkers, represent a special subcategory of MOF–polymer composites (Figure 1). In reports of polyMOFs, it was noted that the spacer length between adjacent linker groups along the polymer backbone can play a significant role in determining the properties of the resulting MOF, as well as whether a given polymer is capable of assembling into a polyMOF.[7, 8] In a particularly striking case, MOF synthesis using certain polymeric linkers led to morphological and sorptive changes that were indicative of a hierarchical pore structure.[8, 9] While using polymeric linkers to exercise structural and functional control over MOFs is a promising avenue for expansion of the MOF field, these materials remain relatively understudied in part due to practical difficulties associated with their study. Synthesis and

purification of polymeric MOF linkers can be nontrivial, and few polyMOFs have been described based on existing MOF structures. These two factors make it difficult to develop structure–activity relationships (SARs) relating polymer composition to MOF function. Within this context, an oligomeric model system comprising two or three ligand units (e.g., terephthalic acid, 1,4-benzenedicarboxylic acid, H_2bdc) bridged by alkyl tethers of varying lengths (e.g., 5-8 methylene repeat units) presents an opportunity to understand polyMOFs, as well as the intermediate structures between molecular MOFs and polyMOFs (Figure 1).

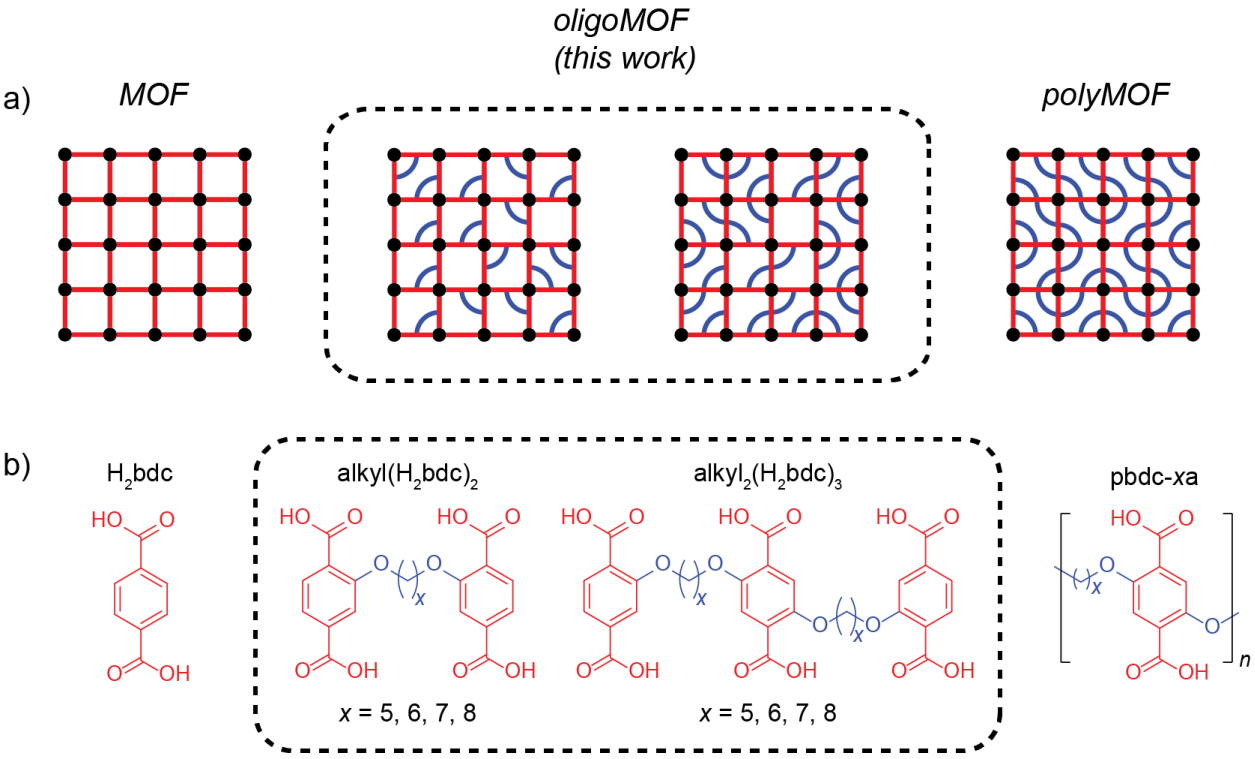

Figure 1. (a) Schematic representation of oligomeric-linker MOFs (oligoMOFs) compared to molecular MOFs and polyMOFs. (b) Monomeric, oligomeric, and polymeric H_2bdc linkers (ligands).

Oligomeric MOFs have been previously described. Terephthalic acid dimers and trimers with alkyl or aryl spacer groups have been used to synthesize analogs of IRMOF-1 (IRMOF = isoreticular metal-organic framework 1; a.k.a., MOF-5).[10, 11] The He group crosslinked the linker precursor of NOTT-101 (terphenyl-3,3'',5,5''-tetracarboxylic acid) using a 1,3-dioxypropyl spacer group, and used the resulting dimeric ligand to synthesize an isostructural MOF ZJNU-80, which showed modified uptake behavior of 2-butene with minimal changes in uptake of smaller sorbates (CH_4, N_2, CO_2).[12] The Zhou group crosslinked aldehyde-decorated imidazole ligands and incorporated them into ZIF-8 via postsynthetic linker exchange (PSE), followed by hydrolysis of these dimers to yield free aldehyde groups with controlled distribution throughout the framework.[13] Dong, Guan, and coworkers synthesized an amide-tethered aminoterephthalic acid dimer and used this species to grow a crosslinked shell on UiO-66, leading to enhanced CO_2/CH_4 uptake selectivity.[14] Recently, Xiao and co-workers crosslinked 4,4''-dioxido-[1,1':4',1''-terphenyl]-3,3''-dicarboxylic acid to generate dimers connected via ester linkages, which could be thermolyzed to yield free carboxylic acids with precise positioning in an expanded MOF-74-type framework.[15] Beyond these simple dimeric and trimeric linker species, Johnson and co-workers have also synthesized several dimeric and tetrameric MOF linkers bridged by or decorated with polymers, which were used to make IRMOF-1 analogs.[16, 17] While these studies demonstrate several potential strategies and uses of oligomeric MOFs, they generally have not explored the relationship between ligand structure and the resulting oligoMOF properties, in particular, by comparison to the molecular and polymeric MOFs. Herein, the ability of oligomeric ligands to assemble into the prototypical IRMOF-1 structure is reported, and oligomeric-linker MOFs (oligoMOFs) are systematically characterized with respect to their synthesis conditions,

crystallinity, accessible internal surface area and porosity, defectivity, and thermal and moisture stability.

RESULTS AND DISCUSSION

Synthesis and Activation. A series of oligomeric dimer and trimer ligands based on the 1,4-benzene dicarboxylic acid (H_2bdc, terephthalic acid) ligand were prepared using standard synthetic approaches (Figure 1, see Supporting Information for details). OligoIRMOF-1, the oligomeric derivative of the canonical IRMOF-1, was successfully prepared with DMF as the synthesis solvent using all the oligomeric linkers listed in Figure 1. In each case, the oligoMOF products (designated as IRMOF-1-alkyl$(bdc)_2$ for dimers and IRMOF-1-alkyl$_2(bdc)_3$ for trimers, where 'alkyl' indicates the spacer length) were isolated as clear, colorless cubic crystals that coat the walls of the synthesis vessel (Figure S1). Powder X-ray diffraction (PXRD) of these crystals reveals the powder pattern is indicative of an non-interpenetrated IRMOF-1 lattice (Figure 2). Previous reports of IRMOF-1 constructed from oligomeric[10] and polymeric[7] linkers activated these materials from $CHCl_3$ at 105 °C. OligoIRMOF-1 samples in this study were activated from CH_2Cl_2 at 25 °C, which gave lower levels of residual guest species and higher surface areas. Notably, the surface areas measured for all of these species (~2000 m^2 g^{-1}, vide infra) are higher than would be expected for interpenetrated IRMOF-1 (600–1100 m^2 g^{-1}),[18] further validating that the non-interpenetrated framework is synthesized under these conditions.

^{1}H NMR spectra of the digested oligoMOFs show that the oligomeric linkers are preserved during MOF synthesis (Figures S2-S10). The synthesis of standard, molecular IRMOF-1 from H_2bdc (Figure 1) is relatively low yielding (22 – 31% based on H_2bdc). By contrast, oligomeric

linkers gave 80–95% yields of the corresponding oligoIRMOF-1 species (Table S1). This enhanced yield can be attributed to something akin to the chelate effect inherent to oligomeric linkers. Relative to a monomeric linker, the dimer and trimer linkers have the potential for 2–3× more coordination interactions with the growing framework, which is expected to lead to stronger linker association (thermodynamic effect), along with faster linker recruitment and a greater barrier for bound linker to dissociate from the growing MOF due to tethering effects (kinetic effect). Therefore, the increased yield of oligoIRMOF-1 materials compared to molecular IRMOF-1 is tentatively attributed to the oligomeric nature of the linkers, resulting from both kinetic and thermodynamic factors.

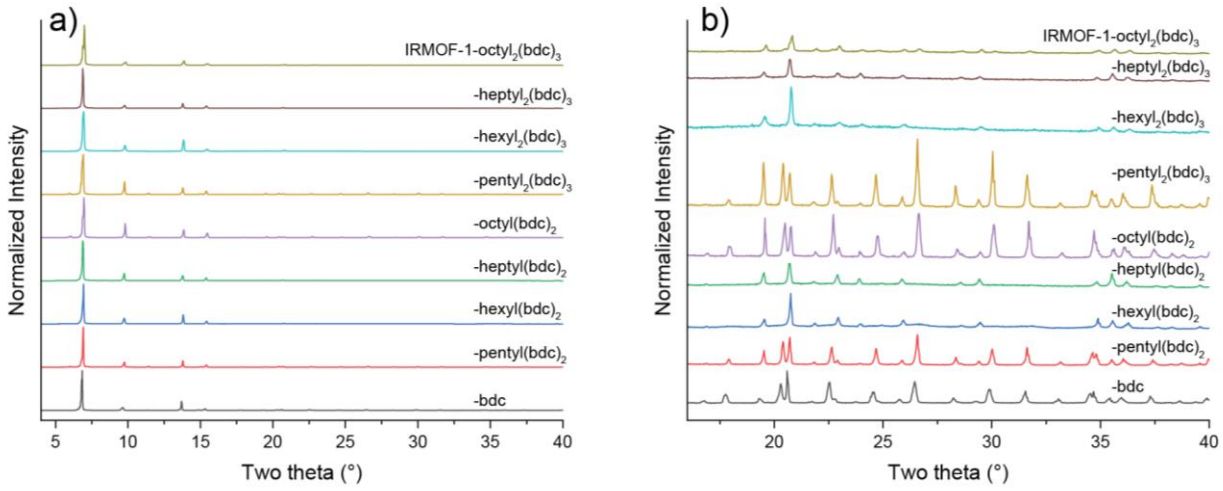

Figure 2. PXRD patterns of IRMOF-1 synthesized with H_2bdc and with alkyl-spaced H_2bdc dimers and trimers. 2θ Range: (a) 4–40° and (b) 16–40°.

The ability of oligomeric linkers to generate non-interpenetrated oligoIRMOF-1 in DMF differs from the reaction outcome with monomeric H_2bdc, which instead yields the interpenetrated

form of the MOF in this solvent.[19] For this reason, the larger and considerably more expensive (~\$600 L^{-1} vs. ~\$35 L^{-1} from Fisher Scientific) formamide solvent *N,N*-diethylformamide (DEF) is generally used to synthesize high quality IRMOF-1. It is notable that the synthesis of interpenetrated IRMOF-1 in DMF, as with the synthesis of the non-interpenetrated form in DEF, also gives a lower yield (75%) than any of the oligoIRMOF-1 syntheses performed here (Table S1). The compatibility of these oligomeric H_2bdc ligands with DMF in the synthesis of oligoIRMOF-1 can be explained by considering the mechanism by which DEF favors non-interpenetrated IRMOF-1: as a larger solvent, DEF acts as a molecular template for the framework and prevents growth of interpenetrating phases.[19] The alkyl chains in the linker oligomers appear to serve the same purpose in these syntheses by providing sufficient steric bulk to prohibit interpenetration. While IRMOF-1 analogs were synthesized in DMF in previous studies with both oligomeric[10, 11] and polymeric[7, 20] H_2bdc, the ability of crosslinked MOF linkers to disfavor interpenetration is a heretofore unrecognized synthetic benefit.

Crystallinity and Accessible Porosity. The oligoIRMOF-1 samples demonstrate excellent crystallinity and high accessible surface areas. PXRD patterns of oligoIRMOF-1 samples show minimal low-angle deviations from the powder pattern associated with standard, non-interpenetrated IRMOF-1 (Figure 2a), other than peak shifting indicative of a ~0.5% unit cell contraction (Figure S11). However, oligoIRMOF-1 samples created from the hexyl- and heptyl-spaced linker oligomers lose all reflections with odd *h*, *k*, or *l* values from their diffraction patterns (Figure 2b). This observation suggests that the framework has increased its symmetry from $Fm\bar{3}m$ to $Pm\bar{3}m$ with halved lattice parameters, as the orientation of the tetrametric basic zinc carboxylate $Zn_4O(OOCR)_6$ clusters are disordered over two positions, rather than alternating throughout the structure. The relative orientation of these clusters is controlled by the dihedral angles of the linker

carboxylate groups: in IRMOF-1 the ligand can adopt a planar configuration that is not achieved in oligoIRMOF-1 with hexyl or heptyl spacers. This loss of cluster orientational coherence is also seen in other IRMOFs with bulkier ethereal substituents,[21, 22] including the polyMOF Zn-pbdc-7a.[7] There is significant diffuse scattering confined to planes normal to the ⟨100⟩ directions for all samples (Figures S12-S13), suggestive of strong short-range correlations between the orientations of the Zn_4O clusters. These diffraction data demonstrate that, while all of these samples display long-range crystallinity comparable to that of the parent framework, spacer length is an important parameter in dictating cluster orientational coherence in oligoIRMOF-1.

The change in Zn_4O cluster orientations observed in oligoIRMOF-1 was further investigated from computationally. In order to analyze the preference of each spacer length for different cluster orientations, IRMOF-1 structures with alternating and non-alternating clusters were prepared (Figure S14). Next, the chemical structures of the dimers (from pentyl- to octyl-) were optimized and their possible locations within the oligoIRMOF-1 structures were evaluated (Figure S15). For all of the possible orientations where insertion was feasible, the total DFT energies were computed for comparison purposes. The energetic differences for each dimer in each possible orientation are summarized in Table S2. Out of the four dimers analyzed, the pentyl-spaced dimer was found to be exceptionally stable in the standard IRMOF-1 alternating cluster configuration compared to the analogous non-alternating structure. This is consistent with the experimental result that both pentyl-spaced oligoIRMOF-1 samples (based on pentyl dimers and trimers, Figure 2b) showed minimal differences in their PXRD patterns from IRMOF-1.

Consistent with their high crystallinity, oligoIRMOF-1 samples synthesized from these H_2bdc dimers and trimers show no changes in their N_2 sorption isotherm shape relative to the parent framework (Figure S16), but a decrease in total N_2 uptake is observed, with longer tethers

generally correlating with lower uptake. BET surface areas of the oligoIRMOF-1 samples decrease from ~3580 m^2 g^{-1} for IRMOF-1 to ~2200 m^2 g^{-1} (61% of IRMOF-1) for the dimer samples and as low as ~1900 m^2 g^{-1} (53% of IRMOF-1) for the trimer samples (Table 1). Unsurprisingly, longer spacers were associated with greater reductions in surface area. Additional structural information can be gleaned from comparison of pore size distributions of these materials (Figure S17). The parent, molecular IRMOF-1 framework predominantly contains a single pore size (~12–14 Å) as previously reported.[23, 24] The pores of IRMOF-1-pentyl(bdc)$_2$ show greater size dispersity, ranging from 9.5–14 Å, consistent with pore contraction/distortion induced by the bridging alkyl groups. Within the hexyl–octyl dimeric oligoIRMOF-1 samples, the pores are further constricted to a narrower size range (9.5–12.5 Å), and a population of 8.0 Å pores are observed that become more prominent with longer tethers. A similar pore contraction effect is observed with increasing tether length in the trimeric oligoIRMOF-1 samples. Taken together, these PXRD and sorption data indicate that the IRMOF-1 topology is highly tolerant of oligomeric linkers, as evidenced by excellent retention of long-range crystallinity and accessible surface areas, even when utilizing alkyl spacers that induce crystallographic symmetry changes and pore contraction in the MOF.

Table 1. BET surface areas of oligoIRMOF-1 and percent surface area relative to the parent, molecular IRMOF-1.

Linker	**Surface area (m^2 g^{-1})[a]**	**Relative surface area (% of IRMOF-1)**
H_2bdc	3580 ± 10	100
pentyl(H_2bdc)$_2$	2310 ± 20	65

hexyl(H_2bdc)$_2$	2270 ± 20	63
heptyl(H_2bdc)$_2$	2240 ± 10	63
octyl(H_2bdc)$_2$	2160 ± 30	60
pentyl$_2$(H_2bdc)$_3$	2080 ± 10	58
hexyl$_2$(H_2bdc)$_3$	1990 ± 90	56
heptyl$_2$(H_2bdc)$_3$	1920 ± 30	54
octyl$_2$(H_2bdc)$_3$	1760 ± 10	49

[a] Error is given as standard error of the mean (n = 3).

Defectivity. ^{1}H NMR spectroscopy of digested, activated oligoIRMOF-1 samples reveals the presence of greater quantities of DMF and formate/formic acid (FA) than is observed in molecular IRMOF-1 (Table 2, Figures S2-S10, see Supporting Information for details). Trimeric oligoIRMOF-1 samples generally contain an increased proportion of residual guests relative to dimeric oligoIRMOF-1 samples with the same tether length. The pentyl-tethered samples show the greatest proportion of residual guests, with 4.6 and 4.2 DMF molecules and 2.9 and 4.0 FA molecules per 100 H_2bdc units for the dimeric and trimeric samples, respectively. This observation cannot be explained through consideration of relative crystallinity, accessible surface area, or pore sizes, as the pentyl oligomer IRMOF-1 samples exceed or match the other samples in these metrics. The greater guest content of the pentyl-tethered oligoIRMOF-1 samples instead suggests hindered diffusion through these frameworks, likely due to more restricted pore apertures. The shorter pentyl spacer has fewer degrees of freedom than the longer spacer groups, perhaps giving it greater rigidity. As the spacer group increases in length, greater spacer flexibility appears to lead to more efficient solvent exchange and removal, particularly in the case of DMF. In contrast, the quantity of residual FA does not trend with spacer length. FA may exist in the MOF as formate ions that

coordinate Zn(II) at the framework secondary building units (SBUs). In this case, these data suggest that the pentyl and octyl spacers lead to more missing linker sites than the hexyl and heptyl spacers.

Table 2. Residual DMF and FA in oligomeric-linker IRMOF-1 determined by ^{1}H NMR. Values are expressed as the number of guests per 100 H_2bdc units.

Linker	**DMF**[a]	**FA**[a]
H_2bdc	0.08 ± 0.02	0.22 ± 0.07
pentyl(H_2bdc)$_2$	4.6 ± 0.4	2.9 ± 0.2
hexyl(H_2bdc)$_2$	1.7 ± 0.2	0.30 ± 0.08
heptyl(H_2bdc)$_2$	1.3 ± 0.2	0.30 ± 0.02
octyl(H_2bdc)$_2$	0.8 ± 0.2	0.78 ± 0.08
pentyl$_2$(H_2bdc)$_3$	4.22 ± 0.02	4.0 ± 0.1
hexyl$_2$(H_2bdc)$_3$	3.6 ± 0.3	0.56 ± 0.04
heptyl$_2$(H_2bdc)$_3$	2.08 ± 0.04	0.68 ± 0.04
octyl$_2$(H_2bdc)$_3$	1.68 ± 0.02	1.01 ± 0.06

[a] Error is given as standard error of the mean (n = 3).

FTIR bands in molecular IRMOF-1 associated with the–COO^- asymmetric stretch (1610 cm^{-1}, 1508 cm^{-1}) and –COO^- symmetric stretch (1393 cm^{-1}) of the bdc^{2-} ligand are shifted to lower frequencies in oligoIRMOF-1 samples (1605–1607, 1496–1498, 1385–1387 cm^{-1}, respectively; Figure 3). These modest shifts are attributed to electron donation of the alkoxy side groups in the bdc^{2-} oligomers.[25] There is no evidence of large populations of uncoordinated linker –COOH

groups, which can be generally identified by a band at ~1650 cm^{-1},[26] although a shallow stretch at this energy is visible in some of the oligoIRMOF-1 samples (Figure S18).

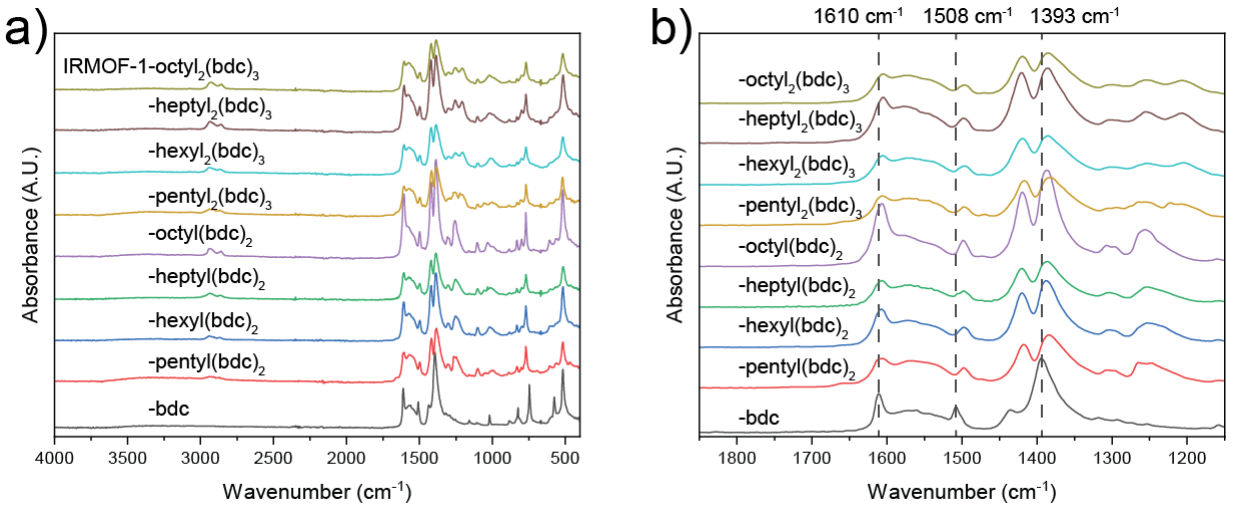

Figure 3. FTIR spectra of oligomeric and parent, molecular IRMOF-1 samples. Wavenumber range: (a) 4000–400 cm^{-1} and (b) 1850–1150 cm^{-1}.

Mass loss evaluation via thermogravimetric analysis (TGA) allows for estimation of the number of linkers present in the MOF per metal cluster (Table S3, see Supporting Information for details). While all but three of the oligoIRMOF-1 samples are within 0.06 of the expected 3 linkers per metal cluster, the three longer trimeric samples are estimated at 3.2–3.4 linkers per cluster. Because these samples do not appear to contain significantly higher quantities of free carboxylic acid as determined by FTIR, this mass loss is hypothesized to result from a population of excess linker in a chemical environment that perturbs its vibrational energy relative to the free, unassociated carboxylic acid (e.g., H-bonded to nearby linkers, metal clusters, water, etc.). The

fact that this excess mass loss is not reflected in any of the other characterization techniques utilized underscores its relatively minor role in dictating the properties of these materials.

Stability. A marked decrease in thermal stability is observed in the oligoIRMOF-1 samples relative to the parent MOF (Figure 4). While the parent, molecular IRMOF-1 material begins to decompose in an aerobic environment at around 410 °C, the decomposition temperature of oligoMOFs is decreased to ~280 °C for nearly all samples. Two exceptions are IRMOF-1-pentyl(bdc)$_2$ and -octyl(bdc)$_2$, which both begin decomposing around 220 °C. The overall lower thermal stability of oligoMOFs likely originates from the reduced thermal stability of the alkane tethers that should expectedly decompose at lower temperatures.

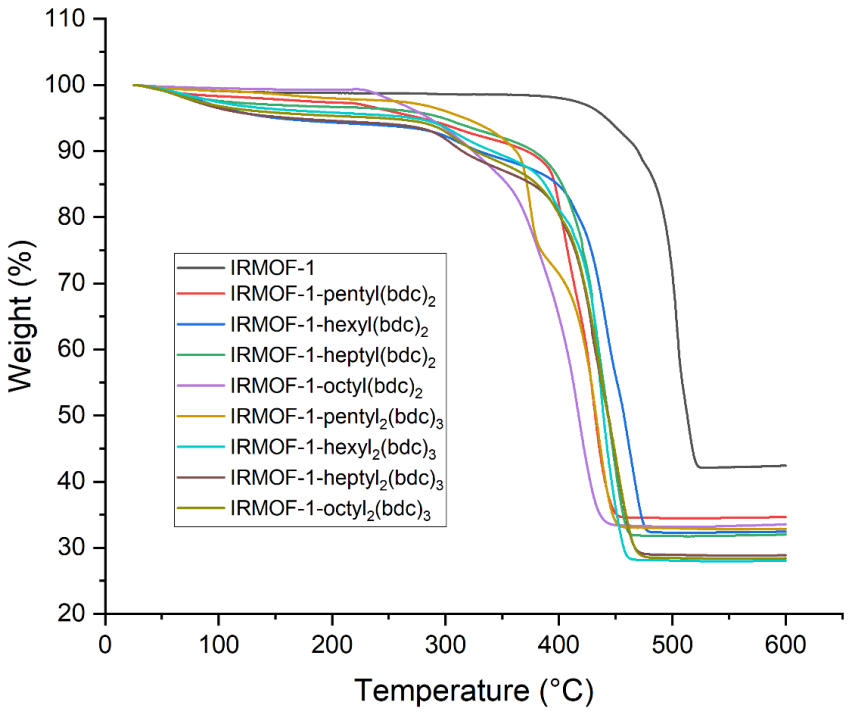

Figure 4. TGA thermograms of parent, molecular IRMOF-1 (black) and oligoIRMOF-1 (colored) samples.

The moisture sensitivity of IRMOF-1 is well-established in the literature.[27] IRMOF-1 analogs with functionalized linkers[28] (including polyIRMOF-1)[7] have shown enhanced hydrolytic stability due to increased hydrophobicity and increased steric bulk around the metal clusters, prompting investigation of the moisture stability of these oligoIRMOF-1 species. To probe the influence of oligomeric linkers on IRMOF-1 atmospheric moisture stability, a set of samples were activated from CH_2Cl_2 at 25 °C, stored in ambient air, and characterized by PXRD to monitor changes in crystallinity. After 12 days of exposure to atmospheric moisture, IRMOF-1 shows complete loss of its original structure (Figure 5a), and converts to a structure with a PXRD pattern that matches $Zn_2(bdc)(OH)_2$ (CCDC reference code: PUCYAO01).[29] By contrast, oligoIRMOF-1 samples demonstrate notably different behavior when stored under these conditions. Use of the oligomeric linkers does not fully mitigate the high humidity degradation observed in the parent IRMOF-1 structure: 5 of the 8 oligomeric samples show complete loss of reflections associated with the MOF, yielding a diffraction pattern characterized by two broad peaks spanning 5–12 and 12–30 °2θ (Figure 5b). The three remaining samples, IRMOF-1-pentyl$(bdc)_2$, -octyl$(bdc)_2$, and -heptyl$_2(bdc)_3$, show these two amorphous peaks to varying degrees, but also retain reflections indicative of the IRMOF-1 lattice. Notably, none of the peaks associated with $Zn_2(bdc)(OH)_2$ are observed in any of the moisture-degraded oligoIRMOF-1 samples, demonstrating the incompatibility of this crystalline phase with the oligomeric linkers.

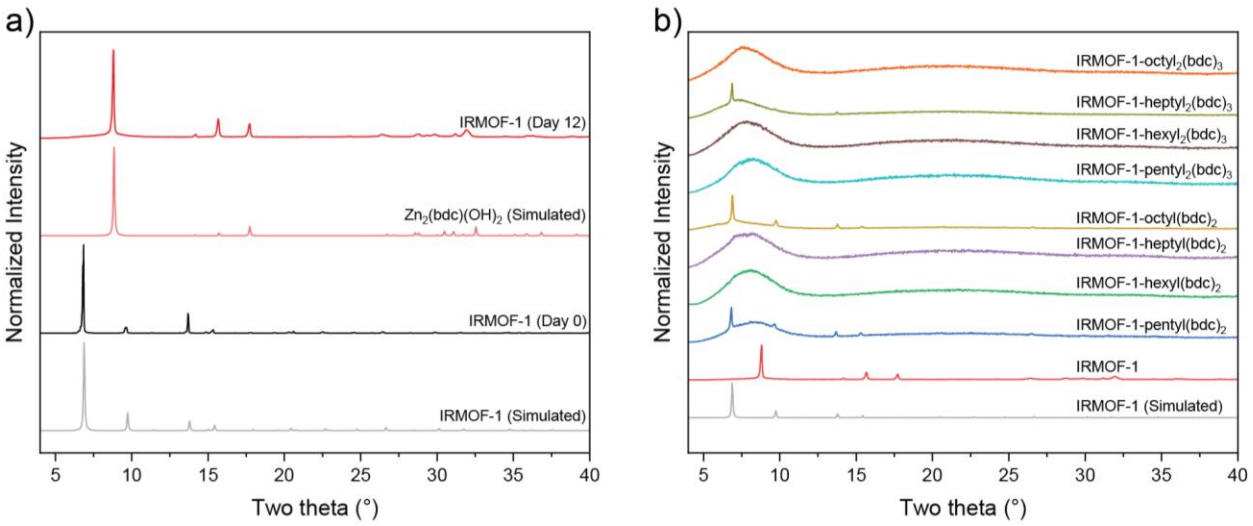

Figure 5. PXRD patterns of IRMOF-1 and oligoIRMOF-1 exposed to ambient air for 12 days. (a) Freshly-activated (black) and 12-day aged (red) IRMOF-1 in ambient air compared to simulated PXRD patterns of IRMOF-1 (gray) and $Zn_2(bdc)(OH)_2$ (pale red). (b) IRMOF-1 (red) and oligoIRMOF-1 after 12 days in ambient air compared to simulated PXRD pattern of IRMOF-1 (gray).

To further probe their stability, a series of activated oligoIRMOF-1 samples were also analyzed after being stored for ~2 months in a desiccator (low humidity conditions). Under these conditions, the parent IRMOF-1 sample does not quantitatively convert to $Zn_2(bdc)(OH)_2$, and instead shows peaks associated with $Zn_2(bdc)(OH)_2$, $Zn(bdc)(H_2O)$ (CCDC reference code: IFABIA)[30] and $Zn(bdc)(H_2O)_2$ (CCDC reference code: DIKQET)[31] (Figure 6a). Under these low humidity storage conditions, beyond a slight increase in the amorphous background signal in IRMOF-1-octyl$(bdc)_2$ (which was also observed when this material was aged in ambient air), no PXRD changes in the oligoIRMOF-1 samples are observed (Figure 6b).

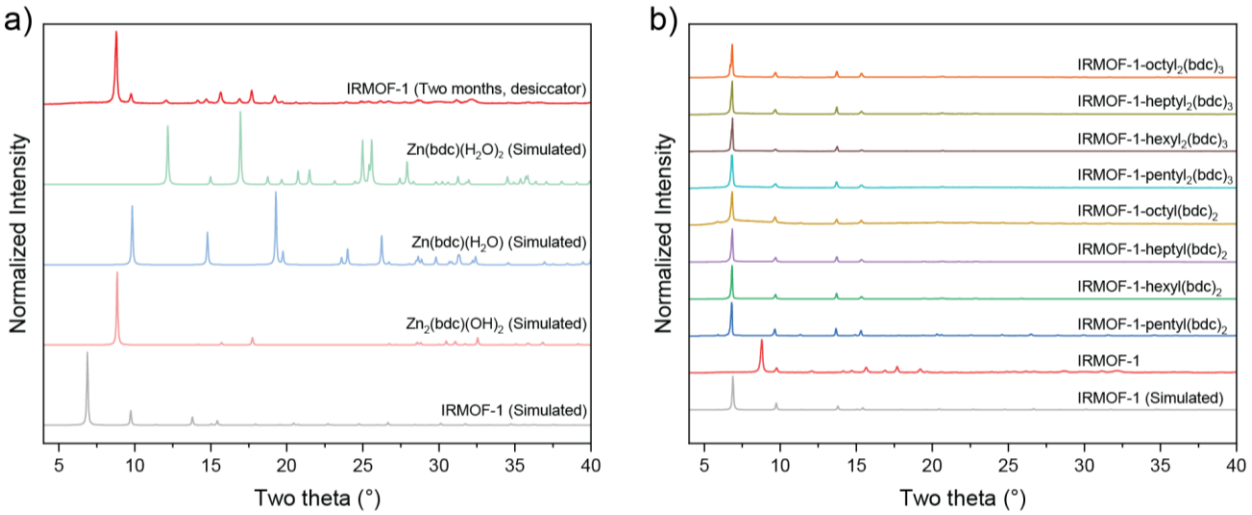

Figure 6. PXRD patterns of IRMOF-1 and oligoIRMOF-1 stored in a desiccator for 2 months. (a) IRMOF-1 aged in a desiccator for 2 months (red) compared to simulated PXRD patterns of IRMOF-1 (gray), $Zn_2(bdc)(OH)_2$ (pale red), $Zn(bdc)(H_2O)$ (pale blue), and $Zn(bdc)(H_2O)_2$ (pale green). (b) IRMOF-1 (red) and oligoIRMOF-1 after 2 months in a desiccator compared to simulated PXRD pattern of IRMOF-1 (gray).

Encouraged by the apparent complete, or near complete, retention of crystallinity, surface areas for desiccator-aged oligoIRMOF-1 samples were measured (Table 3). Pleasingly, most samples retained the majority of their starting surface area (90 – 99%), with only two samples (IRMOF-1-hexyl$(bdc)_2$ and IRMOF-1-hexyl$_2(bdc)_3$) losing nearly all of their accessible surface area, and one (IRMOF-1-octyl$_2(bdc)_3$) losing approximately two-thirds of its original surface area. This retention of bulk crystallinity with loss of accessible surface area is likely due to crystal surface collapse,[32] wherein the outer layer of the MOF degrades and densifies, preventing intrusion of additional water that would degrade the bulk crystallinity of the material. Taken together, these data demonstrate enhanced water stability of oligoIRMOF-1 relative to the parent framework. While the oligoIRMOF-1 samples investigated here are not fully moisture resistant, they display

greatly improved retention of crystallinity and fully suppressed formation of typical IRMOF-1 hydrolysis products. Of the spacers tested, the hexyl spacer is the least effective for maintaining oligoIRMOF-1 accessible surface area in low-humidity environments, while the pentyl and heptyl spacers give nearly full retention of the starting oligoIRMOF-1 surface area (Table 3).

Table 3. BET surface areas of oligomeric-linker IRMOF-1 aged in a desiccator for 2 months and percent surface area relative to the corresponding freshly-activated oligoIRMOF-1.

Linker	**Surface Area (m^2 g^{-1})**	**Retained Surface Area (%)**
pentyl$(bdc)_2$	2273	98
hexyl$(bdc)_2$	34	~1
heptyl$(bdc)_2$	2018	90
octyl$(bdc)_2$	1973	92
pentyl$_2(bdc)_3$	1816	88
hexyl$_2(bdc)_3$	11	<1
heptyl$_2(bdc)_3$	1963	99
octyl$_2(bdc)_3$	572	32

CONCLUSIONS

Using simple and readily synthesized ligands, this work demonstrates the wide tolerance of the IRMOF-1 framework for accommodating oligomeric ligands and the role that tether length plays in dictating the properties of resulting oligoIRMOF-1 materials. Of the four tether lengths examined, the hexyl and heptyl spacers induced a symmetry reduction in IRMOF-1, likely through

strain-induced disorder. However, in all cases, highly crystalline samples with excellent surface areas were generated. Despite the fact that the synthesis of IRMOF-1 in DMF yields an interpenetrated form of the MOF, syntheses of oligoIRMOF-1 in DMF led to preferential formation of the non-interpenetrated MOFs with no other synthetic modifications. The ability of oligomeric linkers to template formation of non-interpenetrated MOF phases is a valuable feature of these species which was previously unreported. MOF yield was also greatly improved by use of oligomeric linkers, which can be explained through a similar principle to the chelate effect, involving both kinetic and thermodynamic factors.

The majority of oligoIRMOF-1 showed greater stability by low humidity degradation, likely through a combination of increased hydrophobicity of the framework and kinetic slowing of water molecule intrusion. Of the tested oligoIRMOF-1 materials, the hexyl-tethered species led to the greatest surface area loss upon storage in a low humidity desiccator. However, in all cases of low humidity degradation of oligoIRMOF-1 materials, bulk crystallinity was maintained, indicating surface collapse with retention of core crystallinity. When aged in humid air, the oligoIRMOF-1 samples showed a different degradation fate than the parent framework due to geometric constraints imposed by the linkers, which prevent formation of the typical crystalline degradation products.

Relative to polyIRMOF-1,[7] the oligoIRMOF-1 samples studied here are considerably more crystalline, and show less PXRD peak broadening with no evidence of amorphous byproducts. In previous studies, heptyl and octyl tethered polyIRMOF-1 samples showed greater crystallinity and phase purity than the pentyl or hexyl materials,[7] and heptyl-tethered polyIRMOF-1 in particular was found to be more geometrically relaxed than either the hexyl and octyl analogs.[20] In contrast, the hexyl- and heptyl-tethered dimeric and trimeric oligoIRMOF-1 samples studied here show

geometric distortions that are not observed in the pentyl or octyl tethered materials. Additionally, polyIRMOF-1 samples synthesized with shorter pentyl and hexyl tethers are characterized by markedly low accessible surface areas (232 and 70 $m^2 g^{-1}$, respectively),[7] while the oligoIRMOF-1 materials described here generally shows higher surface areas with shorter tether lengths (Table 1). While tether length changes induce structural changes in both oligo- and polyMOFs, these comparisons suggest that the number of H_2bdc repeat units and the additional constraints imposed by a polymer linker also plays a major role in dictating structural properties, and that longer oligomeric linkers are likely necessary to better model the emergent behavior of polyMOFs. The findings herein will enable future work seeking to better understand the structure-function relationships present in other oligomeric- and polymeric-linker MOFs, and shed light on an underutilized strategy for structural control and installation of additional functionality in known MOF systems.

EXPERIMENTAL SECTION

General. Starting materials and solvents were purchased and used without further purification from commercial suppliers (Sigma-Aldrich, Alfa Aesar, TCI, Cambridge Isotope Laboratories, Inc., and others). Dimethyl 2-hydroxyterephthalate[33] and dimethyl 2,5-dihydroxyterephthalate[34] were synthesized according to literature procedures. Detailed syntheses of each oligomeric MOF linker are provided in the electronic Supporting Information.

Preparation of IRMOF-1-alkyl(bdc)$_2$ and IRMOF-1-alkyl$_2$(bdc)$_3$. A modified literature procedure was utilized for synthesis of oligoIRMOF-1 materials.[35] $Zn(NO_3)_2 \cdot 6H_2O$ (410mg, 1.38 mmol) and linker (0.36 mmol with respect to H_2bdc units) were dissolved in 10 mL of DMF in a scintillation vial (20 mL). The vial was placed in an oven preheated to 100 °C for 16 h, after which the vial was removed and allowed to cool to room temperature. The supernatant solution was removed and replaced with an equal volume of fresh DMF three times, with 30 min of soaking in DMF between washes. The MOFs were then washed in an identical fashion with CH_2Cl_2. Following the final CH_2Cl_2 wash, MOF samples were activated under vacuum at 25 °C for 16 h prior to analysis. For comparative studies, parent, molecular IRMOF-1 was prepared in an analogous fashion, with H_2bdc as the ligand source and DEF as the synthesis solvent (instead of DMF).

N_2 Sorption Isotherm Analysis. Approximately 50 – 100 mg of dried MOF (bulk solvent removed on a vacuum line for 10 min) was added to a preweighed sample tube and degassed on a Micromeritics ASAP 2020 Adsorption analyzer at 25 °C for 16 h, and the sample tube was then reweighed to determine the sample mass. N_2 sorption was then performed at 77 K on the same instrument. BET surface areas were determined from sorption isotherms using the BETSI

program[36] and pore size distributions were calculated via DFT methods using MicroActive (Version 5.02, Micromeritics).

PXRD Analysis. Powder X-ray diffraction (PXRD) was performed in ambient conditions on a Bruker D8 Advance X-ray diffractometer (40 kV, 40 mA) with Cu Kα radiation (λ = 1.5418 Å) using a LynxEye detector. A scan speed of 0.5 s/step, a step size of 0.02 ° 2θ, and a 2θ range of 5−40 ° were utilized. Approximately 10 mg of activated MOF samples were used for PXRD analyses. Samples were ground with a pestle and mortar to minimize preferred orientation effects.

Digestion and Analysis by ^{1}H NMR. Approximately 5 mg of activated MOF was digested in a mixture of 550 μL of DMSO-d_6 and 50 μL of 35% DCl in D_2O. ^{1}H NMR spectra were collected on a Varian Mercury Plus spectrometer running at 400 MHz.

Thermal Analysis. Approximately 1-5 mg of activated MOF was used for thermal analyses. Samples were heated under an air atmosphere from room temperature to 600 °C (10 °C/min) in a Mettler Toledo TGA/DSC 1 STARe system.

COMPUTATIONAL SECTION

Structure Optimization. Geometry optimization of alkyl-spaced dimer linkers and MOFs were conducted using the first-principles calculations through density functional theory (DFT). For the optimization of linker molecules, Gaussian 09 program[37] was used with the B3LYP functional[38] and 6-31G basis set. Vienna ab initio simulation package (VASP[39]) was used for the MOF optimization. Projector augmented wave method was used in conjunction with the Perdew-Burke-Ernzerhof (PBE) exchange-correction functional within a generalized gradient approximation

(GGA[40]). The convergence tolerance for the energy and the force were set to 0.0001 eV and 0.02 eV/Å, respectively. The cutoff energy of 600 eV was imposed for the calculation.

ASSOCIATED CONTENT

Supporting Information. The Supporting Information is available free of charge on the ACS Publications website at DOI: X. Additional experimental details and supporting figures: Linker syntheses, MOF syntheses, images of MOF syntheses, ^{1}H NMR of digested MOF samples, MOF synthesis yields, PXRD pattern Pawley refinements, XRD precession images, computational figures, N_2 sorption isotherms, pore size distributions, residual guest ^{1}H NMR calculation, and linker:metal TGA calculations.

AUTHOR INFORMATION

Corresponding Author

*E-mail: scohen@ucsd.edu (S.M.C.).

ORCID

Ryan A. Dodson: 0000-0003-3866-1763

Seth M. Cohen: 0000-0002-5233-2280

Author Contributions

The manuscript was written through contributions of all authors. All authors have given approval to the final version of the manuscript.

Funding Sources

This work was supported by a grant from the Department of Energy, Office of Basic Energy Sciences, Division of Materials Science and Engineering under Award No. DE-FG02-08ER46519.

ACKNOWLEDGMENT

We thank Dr. Yongxuan Su for mass spectrometry sample analysis at the Molecular Mass Spectrometry Facility at U.C. San Diego.

REFERENCES

1. Seth, S.; Matzger, A. J., Metal–Organic Frameworks: Examples, Counterexamples, and an Actionable Definition. *Cryst. Growth Des.* **2017,** *17*, 4043-4048.

2. Kirchon, A.; Feng, L.; Drake, H. F.; Joseph, E. A.; Zhou, H.-C., From fundamentals to applications: a toolbox for robust and multifunctional MOF materials. *Chem. Soc. Rev.* **2018,** *47*, 8611-8638.

3. Tranchemontagne, D. J.; Hunt, J. R.; Yaghi, O. M., Room temperature synthesis of metal-organic frameworks: MOF-5, MOF-74, MOF-177, MOF-199, and IRMOF-0. *Tetrahedron* **2008,** *64*, 8553-8557.

4. Purewal, J. J.; Liu, D.; Yang, J.; Sudik, A.; Siegel, D. J.; Maurer, S.; Müller, U., Increased volumetric hydrogen uptake of MOF-5 by powder densification. *Int. J. Hydrogen Energy* **2012,** *37*, 2723-2727.

5. Ren, J.; Musyoka, N. M.; Langmi, H. W.; Swartbooi, A.; North, B. C.; Mathe, M., A more efficient way to shape metal-organic framework (MOF) powder materials for hydrogen storage applications. *Int. J. Hydrogen Energy* **2015,** *40*, 4617-4622.

6. Kitao, T.; Zhang, Y.; Kitagawa, S.; Wang, B.; Uemura, T., Hybridization of MOFs and polymers. *Chem. Soc. Rev.* **2017,** *46*, 3108-3133.

7. Zhang, Z.; Nguyen, H. T.; Miller, S. A.; Cohen, S. M., polyMOFs: A Class of Interconvertible Polymer-Metal-Organic-Framework Hybrid Materials. *Angew. Chem. Int. Ed.* **2015,** *54*, 6152-7.

8. Ayala, S.; Zhang, Z.; Cohen, S. M., Hierarchical structure and porosity in UiO-66 polyMOFs. *Chem. Commun.* **2017,** *53*, 3058-3061.

9. Ayala, S.; Bentz, K. C.; Cohen, S. M., Block co-polyMOFs: morphology control of polymer–MOF hybrid materials. *Chem. Sci.* **2019,** *10*, 1746-1753.

10. Allen, C. A.; Boissonnault, J. A.; Cirera, J.; Gulland, R.; Paesani, F.; Cohen, S. M., Chemically crosslinked isoreticular metal–organic frameworks. *Chem. Commun.* **2013,** *49*, 3200-3202.

11. Allen, C. A.; Cohen, S. M., Exploration of chemically cross-linked metal-organic frameworks. *Inorg. Chem.* **2014,** *53*, 7014-7019.

12. Jiao, J.; Liu, H.; Bai, D.; He, Y., A Chemically Cross-Linked NbO-Type Metal-Organic Framework: Cage or Window Partition? *Inorg. Chem.* **2016,** *55*, 3974-3979.

13. Feng, L.; Wang, K. Y.; Lv, X. L.; Powell, J. A.; Yan, T. H.; Willman, J.; Zhou, H. C., Imprinted Apportionment of Functional Groups in Multivariate Metal-Organic Frameworks. *J. Am. Chem. Soc.* **2019,** *141*, 14524-14529.

14. Chen, C.; Li, X.; Zou, W.; Wan, H.; Dong, L.; Guan, G., Structural modulation of UiO-66-NH2 metal-organic framework via interligands cross-linking: Cooperative effects of pore diameter and amide group on selective CO2 separation. *Appl. Surf. Sci.* **2021,** *553*.

15. Geary, J.; Wong, A. H.; Xiao, D. J., Thermolabile Cross-Linkers for Templating Precise Multicomponent Metal-Organic Framework Pores. *J. Am. Chem. Soc.* **2021,** *143,* 10317-10323.

16. MacLeod, M. J.; Johnson, J. A., Block co-polyMOFs: assembly of polymer–polyMOF hybrids via iterative exponential growth and "click" chemistry. *Polym. Chem.* **2017,** *8,* 4488-4493.

17. Gu, Y.; Huang, M.; Zhang, W.; Pearson, M. A.; Johnson, J. A., PolyMOF Nanoparticles: Dual Roles of a Multivalent polyMOF Ligand in Size Control and Surface Functionalization. *Angew. Chem. Int. Ed.* **2019,** *58*, 16676-16681.

18. Hafizovic, J.; Bjørgen, M.; Olsbye, U.; Dietzel, P. D. C.; Bordiga, S.; Prestipino, C.; Lamberti, C.; Lillerud, K. P., The Inconsistency in Adsorption Properties and Powder XRD Data of MOF-5 Is Rationalized by Framework Interpenetration and the Presence of Organic and Inorganic Species in the Nanocavities. *J. Am. Chem. Soc.* **2007,** *129*, 3612-3620.

19. Zhang, Z.; Zaworotko, M. J., Template-directed synthesis of metal–organic materials. *Chem. Soc. Rev.* **2014,** *43*, 5444-5455.

20. Mileo, P. G. M.; Yuan, S.; Ayala, S.; Duan, P.; Semino, R.; Cohen, S. M.; Schmidt-Rohr, K.; Maurin, G., Structure of the Polymer Backbones in polyMOF Materials. *J. Am. Chem. Soc.* **2020,** *142,* 10863-10868.

21. Eddaoudi, M.; Kim, J.; Rosi, N.; Vodak, D.; Wachter, J.; O'Keeffe, M.; Yaghi Omar, M., Systematic Design of Pore Size and Functionality in Isoreticular MOFs and Their Application in Methane Storage. *Science* **2002,** *295*, 469-472.

22. Henke, S.; Schmid, R.; Grunwaldt, J.-D.; Fischer, R. A., Flexibility and Sorption Selectivity in Rigid Metal–Organic Frameworks: The Impact of Ether-Functionalised Linkers. *Chem. Eur. J.* **2010,** *16*, 14296-14306.

23. Gamage, N.-D. H.; McDonald, K. A.; Matzger, A. J., MOF-5-Polystyrene: Direct Production from Monomer, Improved Hydrolytic Stability, and Unique Guest Adsorption. *Angew. Chem. Int. Ed.* **2016,** *55*, 12099-12103.

24. Ding, N.; Li, H.; Feng, X.; Wang, Q.; Wang, S.; Ma, L.; Zhou, J.; Wang, B., Partitioning MOF-5 into Confined and Hydrophobic Compartments for Carbon Capture under Humid Conditions. *J. Am. Chem. Soc.* **2016,** *138*, 10100-10103.

25. Yang, Q.; Wang, Y.; Tang, X.; Zhang, Q.; Dai, S.; Peng, H.; Lin, Y.; Tian, Z.; Lu, Z.; Chen, L., Ligand Defect Density Regulation in Metal–Organic Frameworks by Functional Group Engineering on Linkers. *Nano Lett.* **2022**.

26. Smith, S. J. D.; Konstas, K.; Lau, C. H.; Gozukara, Y. M.; Easton, C. D.; Mulder, R. J.; Ladewig, B. P.; Hill, M. R., Post-Synthetic Annealing: Linker Self-Exchange in UiO-66 and Its Effect on Polymer–Metal Organic Framework Interaction. *Cryst. Growth Des.* **2017,** *17*, 4384-4392.

27. Kaye, S. S.; Dailly, A.; Yaghi, O. M.; Long, J. R., Impact of Preparation and Handling on the Hydrogen Storage Properties of Zn4O(1,4-benzenedicarboxylate)3 (MOF-5). *J. Am. Chem. Soc.* **2007,** *129*, 14176-14177.

28. Yang, J.; Grzech, A.; Mulder, F. M.; Dingemans, T. J., Methyl modified MOF-5: a water stable hydrogen storage material. *Chem. Commun.* **2011,** *47*, 5244-5246.

29. Lee, H. K.; Lee, J. H.; Moon, H. R., Mechanochemistry as a Reconstruction Tool of Decomposed Metal–Organic Frameworks. *Inorg. Chem.* **2021,** *60*, 11825-11829.

30. Edgar, M.; Mitchell, R.; Slawin, A. M. Z.; Lightfoot, P.; Wright, P. A., Solid-State Transformations of Zinc 1,4-Benzenedicarboxylates Mediated by Hydrogen-Bond-Forming Molecules. *Chem. Eur. J.* **2001,** *7*, 5168-5175.

31. Rodríguez, N. A.; Parra, R.; Grela, M. A., Structural characterization, optical properties and photocatalytic activity of MOF-5 and its hydrolysis products: implications on their excitation mechanism. *RSC Adv.* **2015,** *5*, 73112-73118.

32. Feldblyum, J. I.; Liu, M.; Gidley, D. W.; Matzger, A. J., Reconciling the Discrepancies between Crystallographic Porosity and Guest Access As Exemplified by Zn-HKUST-1. *J. Am. Chem. Soc.* **2011,** *133*, 18257-18263.

33. Tanabe, K. K.; Allen, C. A.; Cohen, S. M., Photochemical Activation of a Metal–Organic Framework to Reveal Functionality. *Angew. Chem. Int. Ed.* **2010,** *49*, 9730-9733.

34. Song, Q.; Li, Y.; Cao, Z.; Liu, H.; Tian, C.; Yang, Z.; Qiang, X.; Tan, Z.; Deng, Y., Discovery of novel 2,5-dihydroxyterephthalamide derivatives as multifunctional agents for the treatment of Alzheimer's disease. *Biorg. Med. Chem.* **2018,** *26*, 6115-6127.

35. Li, H.; Eddaoudi, M.; O'Keeffe, M.; Yaghi, O. M., Design and synthesis of an exceptionally stable and highly porous metal-organic framework. *Nature* **1999,** *402*, 276-279.

36. Osterrieth, J.; Rampersad, J.; Madden, D. G.; Rampal, N.; Skoric, L.; Connolly, B.; Allendorf, M.; Stavila, V.; Snider, J.; Ameloot, R.; Marreiros, J.; Ania, C. O.; Azevedo, D. C. S.; Vilarrasa-García, E.; Santos, B. F.; Bu, X.; Zang, X.; Bunzen, H.; Champness, N.; Griffin, S. L.; Chen, B.; Lin, R.; Coasne, B.; Cohen, S. M.; Moreton, J. C.; Colon, Y. J.; Chen, L.; Clowes, R.; Coudert, F.; Cui, Y.; Hou, B.; D'Alessandro, D.; Doheny, P. W.; Dinca, M.; Sun, C.; Doonan, C.; Huxley, M.; Evans, J. D.; Falcaro, P.; Riccò, R.; Farha, O. K.; Idrees, K. B.; Islamoglu, T.; Feng, P.; Yang, H.; Forgan, R.; Bara, D.; Furukawa, S.; Sanchez, E.; Gascon, J.; Telalovic, S.; Ghosha, S. K.; Mukherjee, S.; Hill, M. R.; Sadiq, M. M.; Horcajada, P.; Salcedo-Abraira, P.; Kaneko, K.; Kukobat, R.; Kenvin, J.; Keskin, S.; Kitagawa, S.; Otake, K.; Lively, R. P.; DeWitt, S. J. A.; Llewellyn, P. L.; Lotsch, B.;

Emmerling, S. T.; Pütz, A.; Martí-Gastaldo, C.; Muñoz, N.; Garcia-Martinez, J.; Linares, N.; Maspoch, D.; Suarez, J. A.; Moghadam, P.; Oktavian, R.; Morris, R.; Wheatley, P.; Navarro, J.; Petit, C.; Danaci, D.; Rosseinsky, M.; Katsoulidis, A.; Schroder, M.; Han, X.; Yang, S.; Serre, C.; Mouchaham, G.; Sholl, D.; Thyagarajan, R.; Siderius, D.; Snurr, R. Q.; Goncalves, R. B.; Telfer, S. G.; Lee, S. J.; Ting, V.; Rowlandson, J.; Uemura, T.; Iiyuka, T.; van der Veen, M.; Rega, D.; van Speybroeck, V.; Lamaire, A.; Rogge, S.; Walton, K.; Bingel, L. W.; Wuttke, S.; Andreo, J.; Yaghi, O.; Zhang, B.; Yavuz, C.; Nguyen, T.; Zamora, F.; Montoro, C.; Zhou, H.; Angelo, K.; Fairen-Jimenez, D., How Reproducible Are Surface Areas Calculated from the BET Equation? *ChemRxiv* **2021**, doi: 10.26434/chemrxiv.14291644.v2.

37. Frisch, M. J. *et al. Gaussian 09*, Gaussian, Inc: Wallingford CT, 2009.

38. Becke, A. D., Density-functional exchange-energy approximation with correct asymptotic behavior. *Phys. Rev. A* **1988,** *38*, 3098-3100.

39. Kresse, G.; Hafner, J., Ab initio molecular dynamics for liquid metals. *Phys. Rev. B* **1993,** *47*, 558-561.

40. Perdew, J. P.; Burke, K.; Ernzerhof, M., Generalized Gradient Approximation Made Simple. *Phys. Rev. Lett.* **1996,** *77*, 3865-3868.